

Harmonic-Constrained Optimal Modulation for Converters Connected to a Distorted Grid

Shirin Rahmanpour, *Student Member, IEEE*, Petros Karamanakos, *Senior Member, IEEE*, Tobias Geyer, *Fellow, IEEE*, Arttu Ruusila, *Student Member, IEEE*, and George Papafotiou, *Member, IEEE*

Abstract—Compliance with harmonic grid standards becomes particularly challenging under non-ideal operating conditions, e.g., when other converters—besides the one of interest—inject harmonic distortions, referred to as disturbances, at the point of common coupling (PCC). This paper proposes optimized pulse patterns (OPPs) for grid-connected converters with an *LCL* filter that ensure PCC current and voltage harmonics meet the relevant harmonic grid standards, even in the presence of such disturbances. This is achieved by formulating the OPP problem as a robust optimization problem that explicitly accounts for external harmonic distortions and incorporates explicit current and voltage harmonic constraints. The proposed framework can be applied under different levels of disturbance information: (i) full knowledge of harmonic amplitudes and phases, (ii) uncertain but bounded characteristics, and (iii) complete lack of knowledge during the OPP computation. Numerical results and experimental tests demonstrate that the proposed OPPs achieve significantly better compliance with harmonic grid standards compared with advanced modulation strategies such as selective harmonic elimination (SHE) and conventional OPPs.

Index Terms—Grid-connected converters, grid standards, harmonic distortion, *LCL* filter, optimized pulse patterns (OPPs), pulse width modulation (PWM).

I. INTRODUCTION

THE growing adoption of grid-connected converters in distributed generation, including renewable energy sources, poses significant challenges for maintaining power quality in modern electrical networks. These converters inject harmonic distortions at the point of common coupling (PCC), which can adversely affect other grid customers. To preserve overall grid reliability and protect customers from such negative effects, the output current and voltage of grid-connected converters must comply with established grid standards. Standards such as IEEE 519 [1] and IEC 61000-2-4 [2] specify permissible limits on individual harmonics and the total demand distortion (TDD) at the PCC.

Hardware-based approaches for mitigating switching-induced harmonic distortion rely on passive filters, particularly *LCL* configuration. These filters have been widely used to

connect power converters to the grid due to their simplicity and effectiveness in attenuating harmonics above their resonance frequency. However, they provide limited suppression of low-order harmonics, making full compliance with harmonic grid standards challenging. To address this limitation, hybrid strategies that combine passive filters with active power filters (APFs) have been proposed [3]–[5]. Such strategies dynamically compensate for low-order harmonics and improve compliance, but they also increase design complexity and overall system cost.

In contrast, software-based pulse width modulation (PWM) techniques provide a cost-effective means of improving output power quality. Conventional PWM schemes, such as carrier-based PWM (CB-PWM) and space vector modulation (SVM), are widely used due to their straightforward implementation [6]. However, the use of a fixed modulation cycle gives rise to pronounced sideband harmonics around the switching frequency and its integer multiples. If any of these components lies near the resonance frequency of the *LCL* filter, the filter resonance may be excited, leading to a significant rise in current and voltage distortions. Increasing the switching frequency can mitigate this resonance interaction, but at the cost of higher switching losses. This reflects a fundamental limitation of conventional PWM methods, namely an unavoidable trade-off between harmonic performance and conversion efficiency.

To improve this trade-off—which is crucial for achieving both grid- and converter-friendly operation—offline programmed PWM strategies, such as selective harmonic elimination/mitigation (SHE/SHM) [7]–[13], optimized pulse patterns (OPPs) [14]–[18], and hybrid modulation approaches [19], allow the switching instants (referred to as switching angles) to be distributed more freely. This flexibility makes it possible to lower harmonic distortions while also reducing switching losses since operation at lower switching frequencies is possible. In SHE/SHM, the switching angles are computed so that specific harmonics are eliminated/mitigated, ensuring their compliance with harmonic grid standards. Yet, achieving compliance across the entire harmonic spectrum remains challenging, as solving the resulting system of nonlinear equations/inequalities to determine a larger set of switching angles can be computationally intractable and highly sensitive to the accuracy of angles. Moreover, eliminating selected harmonics often redistributes harmonic energy to other frequencies, thereby degrading overall current quality.

OPPs, in contrast, are obtained by solving an optimization problem that minimizes the TDD of the output current, thus

The work of Shirin Rahmanpour and Petros Karamanakos was supported by the Research Council of Finland.

Shirin Rahmanpour, Petros Karamanakos, and Arttu Ruusila are with the Faculty of Information Technology and Communication Sciences, Tampere University, 33101 Tampere, Finland; e-mail: shirin.rahmanpour@tuni.fi, p.karamanakos@ieee.org, arttu.ruusila@tuni.fi

Tobias Geyer is with ABB System Drives, 5300 Turgi, Switzerland; e-mail: t.geyer@ieee.org

George Papafotiou is with the Department of Electrical Engineering, Eindhoven University of Technology, 5612 Eindhoven, the Netherlands; e-mail: g.papafotiou@tue.nl

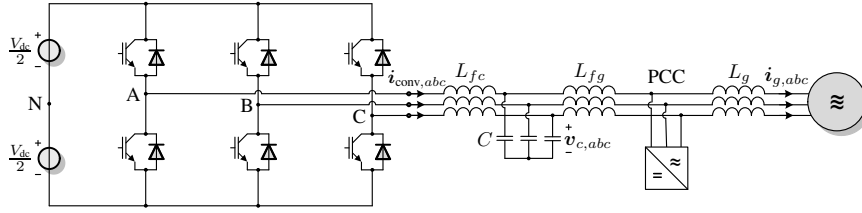


Fig. 1: A two-level converter connected to the grid via an LCL filter and a transformer. Other converters connected to the PCC introduce additional harmonics.

yielding superior harmonic performance. However, since the OPP optimization criterion focuses solely on distortion minimization, compliance with harmonic grid standards is not inherently guaranteed. This limitation was addressed in [20] by extending the OPP formulation for grid-connected converters with an LCL filter to include constraints on individual grid current harmonics, as required by relevant grid standards. Although these harmonic-constrained OPPs ensure compliance with the harmonic grid standards, they are designed under the assumption of an ideal grid, while real grids often contain background harmonic voltages (disturbances) generated by other converters connected to the PCC.

Such disturbances were considered in [21], where the harmonic-constrained OPP problem was further extended to also include harmonic contributions from other converters. Although this approach ensures that current and voltage harmonics at the PCC meet the relevant grid standards, it relies on exact knowledge of the disturbance profile—i.e., the amplitude, phase, and frequency of its harmonics. Such precise information, however, is rarely available in practice. Therefore, even small deviations from the assumed disturbance profile can compromise compliance with harmonic grid standards.

To address the shortcomings of [21], this work introduces a *robust* harmonic-constrained OPP optimization framework that explicitly accounts for the most challenging disturbance scenarios. As a result, the proposed OPPs ensure compliance with harmonic grid standards not only for fully known disturbances, but also for uncertain yet bounded disturbance sets. Furthermore, OPPs can be computed that keep all harmonics within their permissible limits even in the absolute absence of disturbance knowledge. Comprehensive numerical and experimental results demonstrate that the proposed robust OPPs achieve significantly better compliance than conventional OPPs and SHE in the presence of harmonic disturbances at the PCC. In particular, the proposed modulation method guarantees compliance when partial disturbance information is available. Moreover, even without any prior disturbance knowledge, harmonic grid standards are met provided that the amplitudes of the disturbance harmonics are below 50% of their maximum allowable levels, regardless of their phase. Neither conventional OPPs nor SHE exhibit comparable robustness against harmonic disturbances in any of the evaluated scenarios.

The remainder of this article is organized as follows. Section II models grid-connected converters with an LCL filter under disturbances at the PCC. Section III first presents the conventional OPP optimization problem and then introduces the proposed OPP framework that incorporates disturbances,

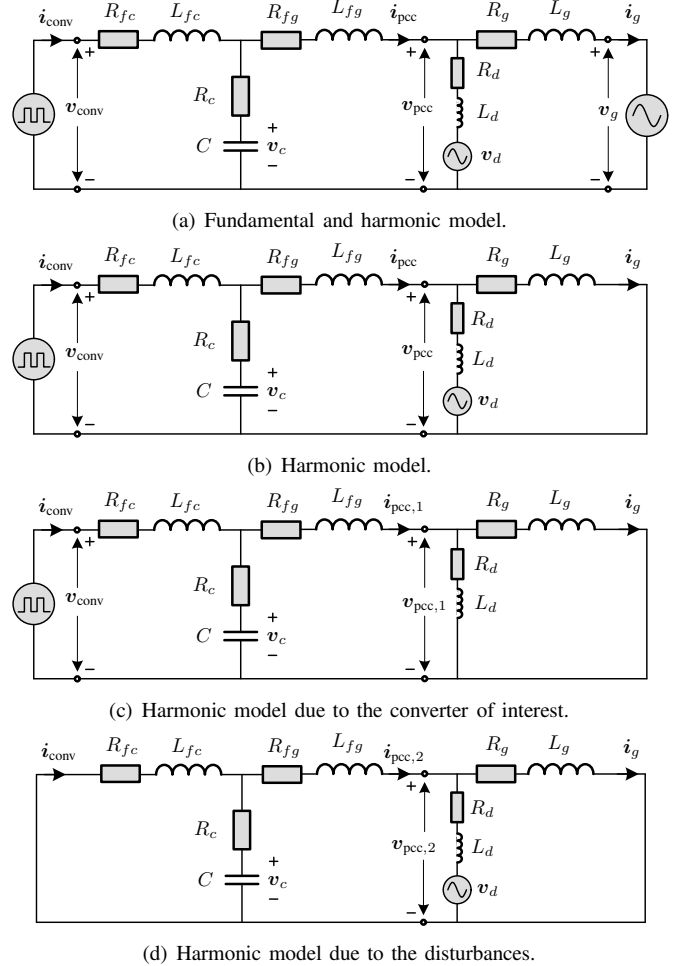


Fig. 2: Equivalent circuit in the stationary orthogonal ($\alpha\beta$) frame.

progressing from full knowledge to complete uncertainty. The performance of the proposed optimal modulation method is benchmarked against conventional OPPs and SHE through numerical and experimental tests in Section IV. Subsequently, Section V discusses the limitations of the proposed modulation method and outlines potential directions for future research. Finally, Section VI concludes the paper.

II. SYSTEM MODEL IN THE PRESENCE OF DISTURBANCES

In this paper, OPPs are designed for a low-voltage (LV) power electronic system consisting of a two-level converter connected to the grid through an LCL filter and a transformer, as illustrated in Fig. 1.¹ In addition to the converter

¹The grid-side filter and transformer inductances are lumped together and represented by L_{fg} .

under study, other converters are assumed to be connected to the same PCC, injecting additional harmonic currents and voltages. To capture these interactions, Fig. 2(a) presents the corresponding $\alpha\beta$ -frame equivalent circuit for both fundamental and harmonic components.² For the subsequent analysis, the harmonic model shown in Fig. 2(b) is employed, where the grid voltage v_g is assumed to be ripple-free and thus short-circuited. The aggregate effect of all external converters connected to the PCC is represented by an equivalent voltage source v_d , connected through a transformer modeled as a series RL branch with lumped inductance L_d and resistance R_d . The harmonics of the voltage across this branch, denoted by $v_{\text{pcc},2}$ (see Fig. 2(d)), are treated as disturbances acting on the system.

To derive the current and voltage harmonics at the PCC, contributions from two distinct harmonic sources must be considered: the converter of interest and the disturbances. The procedure for this derivation is presented in the sequel.

A. Harmonic Contribution of Converter Under Study

To investigate the contribution of the converter, the disturbance source v_d is modeled as a short circuit (see Fig. 2(c)). Under this assumption, circuit analysis of Fig. 2(c) yields the system dynamics in the form of differential equations.³ To this end, the converter current i_{conv} , the converter-contributed PCC current $i_{\text{pcc},1}$, and the capacitor voltage v_c are chosen to form the system state vector, i.e., $[i_{\text{conv}}^T \ i_{\text{pcc},1}^T \ v_c^T]^T \in \mathbb{R}^6$. The system input is the three-phase converter switch position $\mathbf{u}_{abc} = [u_a \ u_b \ u_c]^T \in \{-1, 1\}^3$,⁴ while the system outputs are the three-phase converter-contributed PCC current $i_{\text{pcc},1,abc} \in \mathbb{R}^3$ and voltage $v_{\text{pcc},1,abc} \in \mathbb{R}^3$.

With these definitions, the state-space representation of the system can be obtained, as shown in [21]. Based on this model, the transfer matrices describing the impact of the applied switching signals (pulse patterns) \mathbf{u}_{abc} on the PCC current and voltage are derived in the frequency domain using the Laplace transform. These have the form

$$\begin{aligned} \mathbf{H}_1(s) &= \mathcal{L}\{i_{\text{pcc},1,abc}\}(s)/\mathcal{L}\{\mathbf{u}_{abc}\}(s) \\ \mathbf{H}_2(s) &= \mathcal{L}\{v_{\text{pcc},1,abc}\}(s)/\mathcal{L}\{\mathbf{u}_{abc}\}(s). \end{aligned} \quad (1)$$

B. Harmonic Contribution of Disturbances

In a similar manner, the effect of the disturbances on the system is investigated by modeling the converter under study as a short circuit (see Fig. 2(d)). The state vector is defined as $[i_{\text{conv}}^T \ i_{\text{pcc},2}^T \ v_c^T \ i_g^T]^T \in \mathbb{R}^8$, where $i_{\text{pcc},2}$ denotes the current contributed by the disturbances at the PCC, and i_g is the grid current. The system outputs in this case are the three-phase PCC current and voltage due to the disturbances, i.e., $i_{\text{pcc},2,abc} \in \mathbb{R}^3$ and $v_{\text{pcc},2,abc} \in \mathbb{R}^3$, respectively.

Based on this setup, a state-space model is derived by treating the three-phase disturbance voltage at the PCC $v_{\text{pcc},2,abc}$

²For notational simplicity, variables in the $\alpha\beta$ -frame are written without the corresponding subscript throughout the paper.

³For a detailed derivation of the differential equations, see [21].

⁴The converter output voltage in Fig. 2 is $v_{\text{conv}}(t) = (V_{\text{dc}}/2)\mathbf{K}\mathbf{u}_{abc}(t)$, with V_{dc} denoting the dc-link voltage and \mathbf{K} being the transformation matrix from the abc - to the $\alpha\beta$ -frame.

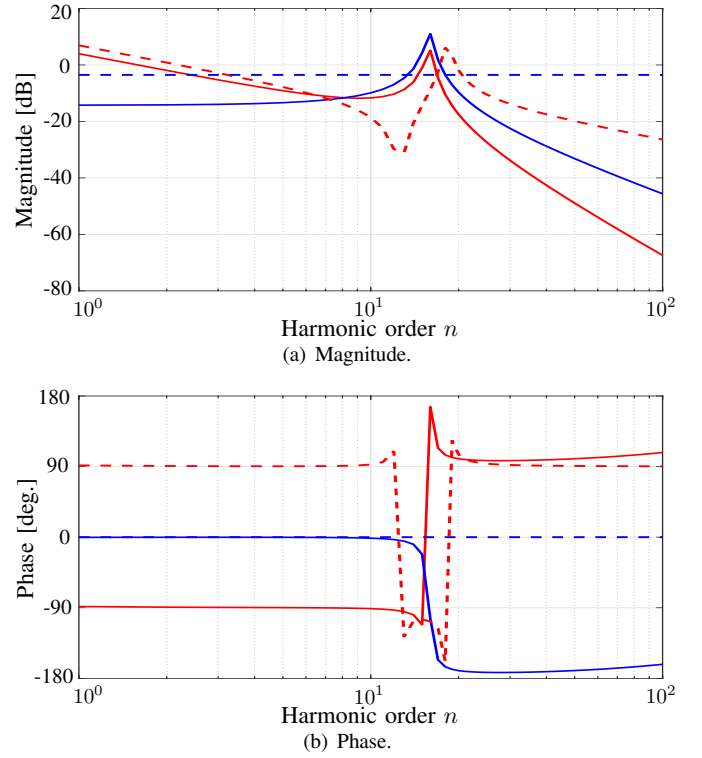


Fig. 3: System transfer functions relating the converter switching signal to the PCC current (red solid line) and voltage (blue solid line), and the disturbance voltage to the PCC current (red dashed line) and voltage (blue dashed line).

as the input. From this model, the transfer matrices $\mathbf{H}_3(s)$ and $\mathbf{H}_4(s)$ are obtained, which quantify how disturbances propagate into the PCC current and voltage, respectively, i.e.,

$$\begin{aligned} \mathbf{H}_3(s) &= \mathcal{L}\{i_{\text{pcc},2,abc}\}(s)/\mathcal{L}\{v_{\text{pcc},2,abc}\}(s) \\ \mathbf{H}_4(s) &= \mathcal{L}\{v_{\text{pcc},2,abc}\}(s)/\mathcal{L}\{v_{\text{pcc},2,abc}\}(s). \end{aligned} \quad (2)$$

C. Total PCC Current and Voltage

Evaluating the transfer matrices (1) and (2) at $s = jn\omega_g$, where ω_g is the grid angular frequency, describes how the n^{th} ($n > 1$) voltage harmonic—whether originating from the converter or from the disturbances—affects the n^{th} harmonic of the PCC current and voltage. Fig. 3 shows the Bode diagrams of the four system transfer matrices \mathbf{H}_k , $k \in \{1, 2, 3, 4\}$, for the system parameters listed in Table II.

To determine the combined effect of the two different harmonic sources, the total PCC current and voltage are obtained by applying the principle of superposition. Accordingly, the three-phase PCC harmonic current in the frequency domain is given by

$$\begin{aligned} i_{\text{pcc},abc}(s) &= i_{\text{pcc},1,abc}(s) + i_{\text{pcc},2,abc}(s) \\ &= \mathbf{H}_1(s) \mathbf{u}_{abc}(s) + \mathbf{H}_3(s) v_{\text{pcc},2,abc}(s), \end{aligned} \quad (3)$$

and the corresponding three-phase PCC harmonic voltage is

$$\begin{aligned} v_{\text{pcc},abc}(s) &= v_{\text{pcc},1,abc}(s) + v_{\text{pcc},2,abc}(s) \\ &= \mathbf{H}_2(s) \mathbf{u}_{abc}(s) + \mathbf{H}_4(s) v_{\text{pcc},2,abc}(s). \end{aligned} \quad (4)$$

These harmonic-domain expressions form the analytical foundation for formulating the OPP optimization problem that

captures the interaction between converter- and disturbance-induced harmonics at the PCC.

III. TWO-LEVEL OPPS FOR GRID-CONNECTED CONVERTERS WITH AN *LCL* FILTER

OPPs are a synchronous PWM method. Therefore, the switching behavior of a two-level converter can be fully described by a single-phase 2π -periodic signal, e.g., $u(\theta) \equiv u_a(\theta)$. Assuming a balanced three-phase system, the switching signals in phases *b* and *c*, i.e., $u_b(\theta)$ and $u_c(\theta)$, respectively, are obtained by phase-shifting $u(\theta)$ by $-2\pi/3$ and $2\pi/3$, respectively.

By imposing quarter- and half-wave symmetry (QaHWS) on $u(\theta)$, it can then be fully characterized by d switching angles $\alpha_i \in [0, \pi/2]$, $i \in \{1, \dots, d\}$, and $d+1$ switch positions u_j , $j \in \{0, 1, \dots, d\}$, within the first quarter of the fundamental period, with the initial switch position $u_0 \in \{-1, 1\}$. Owing to the symmetry properties and periodicity of $u(\theta)$, the PWM signal over one period can be described by the Fourier series

$$u(\theta) = a_0 + \sum_{n=1}^{\infty} (a_n \cos(n\theta) + b_n \sin(n\theta)), \quad (5)$$

with all a_n Fourier coefficients being zero due to QaHWS. As for the b_n coefficients, the imposed symmetry implies that

$$b_n = \frac{4u_0}{n\pi} \left(1 + 2 \sum_{i=1}^d (-1)^i \cos(n\alpha_i) \right), \quad n = 1, 3, 5, \dots \quad (6)$$

The main advantage of QaHWS lies in its simplicity as it significantly reduces the problem size. However, it also artificially limits the degrees of freedom in the optimization process. As shown in [22], dropping quarter-wave symmetry (QWS) expands the feasible solution space of the OPP optimization problem, thus enabling improved harmonic performance for a given number of switching angles.

When only half-wave symmetry (HWS) is imposed, the switching signal is described by $2d+1$ switching angles $\alpha_i \in [0, \pi]$, $i \in \{1, \dots, 2d+1\}$, within the first half of the fundamental period. In this case, both the a_n and b_n Fourier coefficients in (5) are nonzero and given by

$$\begin{aligned} a_n &= -u_0 \frac{4}{n\pi} \sum_{i=1}^{2d+1} (-1)^i \sin(n\alpha_i), \quad n = 1, 3, 5, \dots \\ b_n &= +u_0 \frac{4}{n\pi} \sum_{i=1}^{2d+1} (-1)^i \cos(n\alpha_i), \quad n = 1, 3, 5, \dots \end{aligned} \quad (7)$$

A. Conventional Harmonic-Constrained OPPs

The conventional QaHWS OPPs for grid-connected converters with an *LCL* filter are computed by assuming zero harmonic disturbances at the PCC. The objective is to minimize the TDD of the output (i.e., PCC) current, defined as

$$I_{\text{TDD}} = \frac{1}{\sqrt{2}I_{\text{nom}}} \sqrt{\sum_{n=5,7,\dots} \hat{i}_{\text{pcc},a,n}^2}, \quad (8)$$

where I_{nom} is the nominal rms current and $\hat{i}_{\text{pcc},a,n}$ denotes the amplitude of the n^{th} phase-*a* PCC current harmonic. The

latter is related to the corresponding switching signal harmonic \hat{u}_n via the gain g_n , i.e., $\hat{i}_{\text{pcc},a,n} = g_n \hat{u}_n$, with $\hat{u}_n = |b_n|$ for QaHWS OPPs. Note that triplen current harmonics (i.e., $n = 3, 9, \dots$) are zero in balanced three-phase wye-connected systems with a floating neutral.

Accordingly, the conventional QaHWS OPP optimization problem is formulated as the following non-convex problem

$$\underset{[\alpha_1 \dots \alpha_d]^T}{\text{minimize}} \quad \sum_{n=5,7,\dots} \left(\frac{g_n}{n} \left(1 + 2 \sum_{i=1}^d (-1)^i \cos(n\alpha_i) \right) \right)^2 \quad (9a)$$

$$\text{subject to} \quad b_1 = m \quad (9b)$$

$$0 \leq \alpha_1 \leq \alpha_2 \leq \dots \leq \alpha_d \leq \frac{\pi}{2} \quad (9c)$$

$$u_0 \in \{-1, 1\}, \quad (9d)$$

where (9b) ensures that the fundamental OPP component corresponds to the desired modulation index $m \in [0, 4/\pi]$, while the $d+1$ inequality constraints (9c) enforce ascending order of the switching angles.⁵ A key feature of this formulation is the inclusion of g_n in the objective function to enable the OPP computation for higher-order systems, such as the one considered in this work. This is in contrast to formulations for first-order systems, see [20] for more details.

However, (9) does not inherently guarantee compliance with harmonic grid standards. To address this, constraints on individual non-triplen odd (i.e., $n = 6k \pm 1, k \in \mathbb{N}^+$) PCC current and voltage harmonics are added to (9) to ensure these harmonics remain below their respective limits $\hat{i}_{n,\text{max}}$ and $\hat{v}_{n,\text{max}}$ as dictated by grid standards. These constraints are implemented as soft (rather than hard) constraints to avoid potential infeasibility of the OPP optimization problem, i.e.,

$$\begin{aligned} \hat{i}_{\text{pcc},a,n} &\leq \hat{i}_{n,\text{max}} + \epsilon_{i,n} \\ \hat{v}_{\text{pcc},a,n} &\leq \hat{v}_{n,\text{max}} + \epsilon_{v,n}, \end{aligned}$$

where the slack variables $\epsilon_{i,n}$ and $\epsilon_{v,n}$ relax the limits on the amplitude of the n^{th} phase-*a* PCC current $\hat{i}_{\text{pcc},a,n}$ and voltage harmonic $\hat{v}_{\text{pcc},a,n}$, respectively.

Nevertheless, the grid-friendly operation of these harmonic-constrained OPPs may deteriorate in the presence of disturbances at the PCC. Under such conditions, compliance with harmonic grid standards necessitates incorporating the effect of disturbances into the system model, as described in Section II.

B. OPPs That Account for Harmonic Disturbances

It is assumed that the n^{th} phase-*a* disturbance voltage harmonic has a known amplitude $\hat{v}_{\text{pcc},2,a,n} = \hat{v}_{n,\text{nom}}$ and phase $\phi_{\text{pcc},2,a,n} = \phi_{n,\text{nom}}$. Under this assumption, the phase-*a* disturbance voltage can be expressed as the Fourier series

$$v_{\text{pcc},2,a}(\theta) = \sum_{n=1}^{\infty} (\tilde{a}_n \cos(n\theta) + \tilde{b}_n \sin(n\theta)), \quad (10)$$

⁵A detailed derivation of (9) is provided in [20].

where the Fourier coefficients \tilde{a}_n and \tilde{b}_n are obtained by solving the following system of nonlinear equations

$$\begin{cases} \hat{v}_{\text{pcc},2,a,n} = \sqrt{\tilde{a}_n^2 + \tilde{b}_n^2} \\ \phi_{\text{pcc},2,a,n} = \arctan(\tilde{a}_n/\tilde{b}_n). \end{cases} \quad (11)$$

To enable effective mitigation of disturbances, OPPs with HWS are adopted instead of QaHWS, as HWS allows adjusting the phase of individual OPP harmonics. Given the Fourier series of HWS OPP and disturbance voltage, the amplitude of the n^{th} phase- a PCC current harmonic can be computed from (3) as

$$\begin{aligned} \hat{i}_{\text{pcc},a,n} = & \left(\left(a_n Q_{1,n} + b_n Q_{2,n} + \tilde{a}_n Q_{3,n} + \tilde{b}_n Q_{4,n} \right)^2 \right. \\ & \left. + \left(-a_n Q_{2,n} + b_n Q_{1,n} - \tilde{a}_n Q_{4,n} + \tilde{b}_n Q_{3,n} \right)^2 \right)^{1/2} \end{aligned} \quad (12)$$

and that of the PCC voltage harmonic from (4) as

$$\begin{aligned} \hat{v}_{\text{pcc},a,n} = & \left(\left(a_n Q_{5,n} + b_n Q_{6,n} + \tilde{a}_n Q_{7,n} + \tilde{b}_n Q_{8,n} \right)^2 \right. \\ & \left. + \left(-a_n Q_{6,n} + b_n Q_{5,n} - \tilde{a}_n Q_{8,n} + \tilde{b}_n Q_{7,n} \right)^2 \right)^{1/2}, \end{aligned} \quad (13)$$

where $Q_{\ell,n}$, $\ell \in \{1, 2, \dots, 8\}$, depend on the entries of the matrices $\mathbf{H}_k(s)$, $k \in \{1, \dots, 4\}$ (see (1) and (2)), for each harmonic of order n [21].

Using (12) and (8), the current TDD becomes

$$\begin{aligned} I_{\text{TDD}} = & \underbrace{\frac{1}{\sqrt{2}I_{\text{nom}}}}_c \left(\sum_{n=5,7,\dots} \left(u_0 \frac{-4Q_{1,n}}{n\pi} \sum_{i=1}^{2d+1} (-1)^i \sin(n\alpha_i) \right. \right. \\ & \left. \left. + u_0 \frac{4Q_{2,n}}{n\pi} \sum_{i=1}^{2d+1} (-1)^i \cos(n\alpha_i) + \tilde{a}_n Q_{3,n} + \tilde{b}_n Q_{4,n} \right)^2 \right. \\ & \left. + \left(u_0 \frac{4Q_{2,n}}{n\pi} \sum_{i=1}^{2d+1} (-1)^i \sin(n\alpha_i) \right. \right. \\ & \left. \left. + u_0 \frac{4Q_{1,n}}{n\pi} \sum_{i=1}^{2d+1} (-1)^i \cos(n\alpha_i) - \tilde{a}_n Q_{4,n} + \tilde{b}_n Q_{3,n} \right)^2 \right)^{\frac{1}{2}}, \end{aligned} \quad (14)$$

which can be expressed as $I_{\text{TDD}} = c\sqrt{J_{\text{dist}}}$. Since the constant c is independent of the optimization variables (i.e., switching angles α_i), it does not affect the optimal solution and can be omitted. Thus, J_{dist} forms the objective function of the OPP optimization problem.

Based on the above, the harmonic-constrained HWS OPPs are obtained by solving the following optimization problem that explicitly accounts for disturbances at the PCC

$$\underset{\alpha_H, \epsilon}{\text{minimize}} \quad J_{\text{dist}} + \epsilon^T \mathbf{W} \epsilon \quad (15a)$$

$$\text{subject to} \quad b_1 = m \quad (15b)$$

$$a_1 = 0 \quad (15c)$$

$$0 \leq \alpha_1 \leq \alpha_2 \leq \dots \leq \alpha_{2d+1} \leq \pi \quad (15d)$$

$$\begin{aligned} \hat{i}_{\text{pcc},a,n} & \leq \hat{i}_{n,\text{max}} + \epsilon_{i,n}, \quad \epsilon_{i,n} \geq 0, \\ \forall n = 6k \pm 1, k \in \mathbb{N}_1 \end{aligned} \quad (15e)$$

$$\begin{aligned} \hat{v}_{\text{pcc},a,n} & \leq \hat{v}_{n,\text{max}} + \epsilon_{v,n}, \quad \epsilon_{v,n} \geq 0, \\ \forall n = 6k \pm 1, k \in \mathbb{N}_1 \end{aligned} \quad (15f)$$

$$u_0 \in \{1, -1\}, \quad (15g)$$

where $\alpha_H = [\alpha_1 \dots \alpha_{2d+1}]^T$ is the vector of switching angles. In this problem, constraints (15b) and (15c) enforce a fundamental OPP component with amplitude $m \in [0, 4/\pi]$ and zero phase. In addition, constraints (15e) and (15f) impose limits on non-triplen odd harmonics $n = 6k \pm 1$, with $k \in \mathbb{N}_1 = \{1, \dots, 8\}$, as typically required by grid standards, e.g., [1] and [2]. Moreover, the slack variables, which are part of the optimization variables, are collected in the vector of slack variables $\epsilon = [\epsilon_i^T \ \epsilon_v^T]^T$, where ϵ_i and ϵ_v contain the current $\epsilon_{i,n}$ and voltage $\epsilon_{v,n}$ slack variables, respectively. To facilitate compliance with harmonic grid standards, violations of the soft constraints are strongly penalized through the diagonal weighting matrix $\mathbf{W} \in \mathbb{R}^{32 \times 32}$, where the dimension corresponds to the total number of constrained current and voltage harmonics.

C. Robust OPPs That Account for Bounded Variations in Disturbances

Problem (15) computes OPPs that ensure grid-friendly operation under a fully known disturbance profile, characterized by specific harmonic amplitudes $\hat{v}_{n,\text{nom}}$ and phases $\phi_{n,\text{nom}}$. However, these OPPs may no longer guarantee compliance if the actual disturbances deviate from their nominal values. Such deviations can arise, e.g., due to changes in the impedance between external converters and the PCC (i.e., L_d and R_d in Fig. 2). To accommodate bounded variations in the disturbance profile, the harmonic-constrained OPPs must be equipped with robustness to ensure compliance with harmonic grid standards even when disturbances are only partially known during the offline computation of the OPPs.

A variation of $\pm x\%$ in L_d and R_d affects both the amplitude and phase of the n^{th} nominal disturbance harmonic (green points in Fig. 4). As a result, the amplitude lies within the interval $\hat{v}_{\text{pcc},2,a,n} \in [\hat{v}_{\text{pcc},2,a,n,\text{min}}, \hat{v}_{\text{pcc},2,a,n,\text{max}}]$, while the phase falls in the range $\phi_{\text{pcc},2,a,n} \in [\phi_{\text{pcc},2,a,n,\text{min}}, \phi_{\text{pcc},2,a,n,\text{max}}]$. Together, these bounds define an annular sector Ξ_n , depicted as the dark gray region in Fig. 4. For computational purposes, these continuous intervals are uniformly discretized on a polar grid, with ten equidistant samples along each radius (harmonic amplitude) and an angular resolution of 10° (blue points in Fig. 4). For each sampled amplitude-phase pair, solving (11) yields the corresponding Fourier coefficients \tilde{a}_n and \tilde{b}_n of the n^{th} disturbance harmonic. Because these sampled

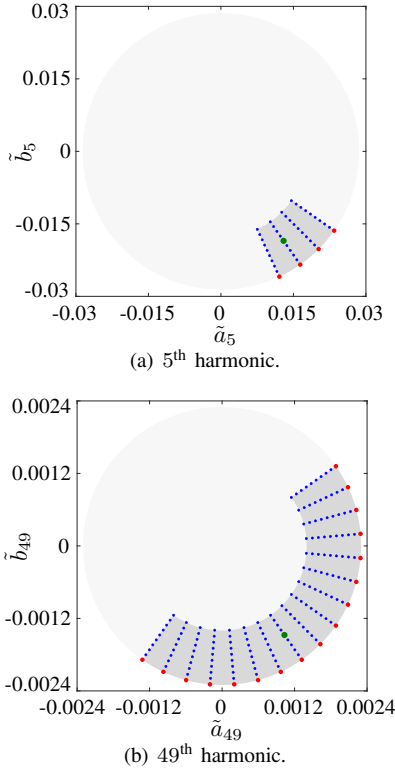


Fig. 4: Uncertainty realizations for the (a) 5th and (b) 49th disturbance voltage harmonics at the PCC. The nominal disturbance is shown in green, while the dark gray region represents all possible realizations under $\pm 25\%$ impedance variations between the external converters and the PCC. Sampled realizations are marked in blue, and the most challenging scenarios are highlighted in red.

pairs represent possible variations in the disturbances, the resulting coefficients are treated as uncertainties in the OPP computation, with each possible pair $\{\tilde{a}_n, \tilde{b}_n\}$ corresponding to one “uncertainty realization.”

For harmonics of order $n = 6k \pm 1$, $k \in \mathbb{N}_1$, every uncertainty realization in Ξ_n must be accounted for to guarantee compliance with harmonic grid standards under disturbance variations. However, evaluating all sampled realizations in Ξ_n would render the corresponding OPP problem computationally intractable. To overcome this while retaining robustness, only those realizations with the maximum amplitude—representing the most challenging scenarios—are kept for each harmonic n .⁶ The resulting reduced uncertainty set $\hat{\Xi}_n$ is an arc of radius $\hat{v}_{\text{pcc},2,n,\text{max}}$ (red points in Fig. 4), with the Fourier coefficients of each considered uncertainty realization collected in the vector $\xi_n = [\tilde{a}_n^T \tilde{b}_n^T]^T$.

Based on these definitions, the proposed robust harmonic-constrained HWS OPPs are computed by solving a min–max optimization problem that minimizes the worst-case current TDD and constraint violations across all realizations in $\hat{\Xi}_n$ for $n = 6k \pm 1$, $k \in \mathbb{N}_1$, i.e.,

⁶The justification for considering only maximum-amplitude realizations is provided in the appendix.

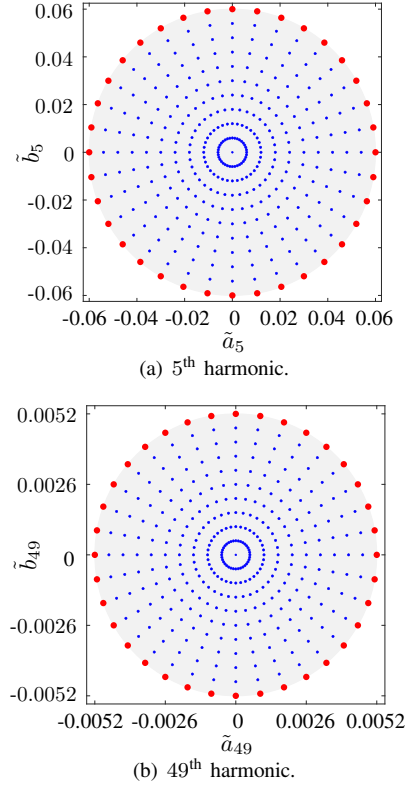


Fig. 5: Uncertainty realizations for the completely unknown (a) 5th and (b) 49th disturbance voltage harmonics at the PCC. The gray region represents all possible realizations in Ξ_n , with sampled realizations shown in blue, and the most challenging realizations highlighted in red.

$$\underset{\alpha_H, \epsilon}{\text{minimize}} \quad \max_{\xi_n \in \hat{\Xi}_n} J_{\text{dist}} + \epsilon^T \mathbf{W} \epsilon \quad (16a)$$

$$\text{subject to} \quad b_1 = m \quad (16b)$$

$$a_1 = 0 \quad (16c)$$

$$0 \leq \alpha_1 \leq \alpha_2 \leq \dots \leq \alpha_{2d+1} \leq \pi \quad (16d)$$

$$\begin{aligned} \hat{i}_{\text{pcc},a,n} &\leq \hat{i}_{n,\text{max}} + \epsilon_{i,n}, \quad \epsilon_{i,n} \geq 0, \\ \forall n = 6k \pm 1, k \in \mathbb{N}_1, \forall \xi_n \in \hat{\Xi}_n \end{aligned} \quad (16e)$$

$$\begin{aligned} \hat{v}_{\text{pcc},a,n} &\leq \hat{v}_{n,\text{max}} + \epsilon_{v,n}, \quad \epsilon_{v,n} \geq 0, \\ \forall n = 6k \pm 1, k \in \mathbb{N}_1, \forall \xi_n \in \hat{\Xi}_n \end{aligned} \quad (16f)$$

$$u_0 \in \{1, -1\}. \quad (16g)$$

D. Robust OPPs That Account for Unknown Disturbances

Although the robust OPP framework in Section III-C accounts for uncertainties in harmonic disturbances, ensuring compliance remains challenging if the disturbance profile is completely unknown at the time of OPP computation. To handle this scenario, the OPP problem in (16) can be further modified, as detailed in the sequel.

When no prior knowledge of the disturbance profile is available, the n^{th} disturbance voltage harmonic is assumed to have an arbitrary phase $\phi_{\text{pcc},2,a,n} \in [-\pi, \pi)$ and an amplitude within the range $\hat{v}_{\text{pcc},2,a,n} \in [0, \hat{v}_{n,\text{max}}]$, where $\hat{v}_{n,\text{max}}$ is specified by the relevant harmonic grid standards. Accordingly, Ξ_n is modeled as a disk of radius $\hat{v}_{n,\text{max}}$ for each $n = 6k \pm 1$,

Algorithm 1 Computation of OPPs Under Disturbances

Input: Desired number of switching angles d ;
Modulation index grid, e.g., $m = 0 : \frac{1}{64\pi} : \frac{4}{\pi}$

- 1: **for** each harmonic $n = 6k \pm 1, k \in \mathbb{N}_1$, **do**
- 2: Define the uncertainty set $\hat{\Xi}_n$ according to the level of disturbance knowledge
- 3: **end for**
- 4: **for** each m in the modulation index grid **do**
- 5: **for** each initial switch position $u_0 \in \{-1, 1\}$ **do**
- 6: Solve problem (16) multiple times using the Matlab function `fmincon` with sequential quadratic programming (SQP) algorithm, each time with a different set of $2d+1$ initial switching angles generated via Halton sequences⁷
- 7: **end for**
- 8: **return** u_0^* and the corresponding switching angles α_H^* that yield the minimum I_{TDD}
- 9: **end for**

$k \in \mathbb{N}_1$ (gray region in Fig. 5). However, to achieve robustness, i.e., compliance under any possible disturbance scenario, it is sufficient to focus only on the most challenging realizations in the reduced set $\hat{\Xi}_n$. This set comprises realizations lying on the circle of radius $\hat{v}_{n,\max}$ for each n (red points in Fig. 5). Solving the OPP problem (16) over these new uncertainty sets yields robust OPPs that facilitate grid-friendly operation under completely unknown disturbance conditions.

It is noteworthy that the proposed OPP framework formulated in (16) adapts to different levels of disturbance knowledge through the definition of the uncertainty set $\hat{\Xi}_n$. Specifically:

- For fully known disturbances, $\hat{\Xi}_n$ reduces to a single point corresponding to the nominal amplitude and phase.
- For bounded variations in a known disturbance profile, $\hat{\Xi}_n$ becomes an arc.
- For completely unknown disturbances, $\hat{\Xi}_n$ forms a full circle.

Finally, the complete procedure for computing the proposed robust OPPs in the presence of PCC harmonic disturbances is outlined in Algorithm 1.

IV. EXPERIMENTAL RESULTS

In this section, the proposed robust OPP framework is evaluated under varying levels of knowledge about harmonic disturbances at the PCC, and benchmarked against conventional QaHWS OPPs—computed with (9)—and SHE. More specifically, three harmonic-constrained HWS OPP types are considered, namely (a) OPPs computed for a fully known disturbance profile via (15) (referred to as disturbance-aware (DA) OPPs), (b) robust OPPs accounting for bounded variations

⁷The evaluations are executed in parallel on the Tampere Center for Scientific Computing (TCSC) cluster by enabling the `UseParallel` option of `fmincon`.

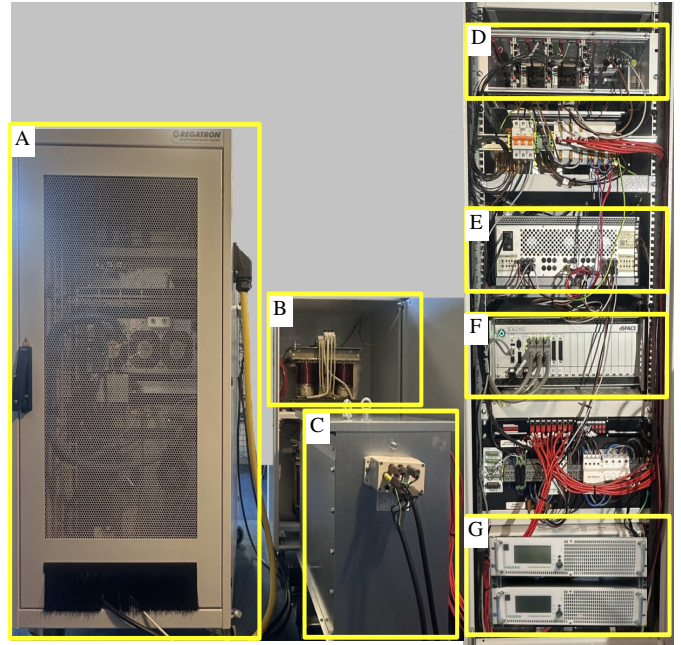


Fig. 6: Experimental setup for a grid-connected converter with an *LCL* filter: (A) grid emulator, (B) three-phase grid impedance, (C) isolation transformer, (D) two-level converter, (E) *LCL* filter, (F) dSPACE SCALEXIO real-time control system, and (G) dc sources.

in the disturbance profile (referred to as robust disturbance-aware (RDA) OPPs), and (c) robust OPPs for completely unknown disturbances (referred to as robust disturbance-agnostic (RDAG) OPPs). All pulse patterns are computed for the LV power electronic system illustrated in Fig. 1.

To validate the performance of these modulation methods, the experimental setup depicted in Fig. 6 is used. It employs a 11 kVA two-level converter built from Imperix PEB8038 power modules. The converter is supplied by stiff dc sources, and connected to the grid through an *LCL* filter with a resonance frequency of 912 Hz, a 400 V transformer providing galvanic isolation, and an inductive load representing the grid impedance. The grid itself is emulated using a Regatron regenerative programmable bidirectional ac power source (model TC.ACS30.528.4WR.S.LC). Since only a single grid emulator is available, the parallel disturbance branch consisting of L_d , R_d , and v_d cannot be physically realized. Instead, disturbances are directly injected via the grid emulator.⁸ The rated values and system parameters of the experimental setup are summarized in Tables I and II, respectively.

The offline-computed switching instants and corresponding switch positions u_{abc} of the considered PWM patterns are stored in lookup tables (LUTs) in the processor of a dSPACE SCALEXIO platform equipped with an Intel i7-6820EQ 2.8 GHz processor and a Xilinx Kintex-7 field-programmable gate array (FPGA). A counter-based mechanism within the FPGA regenerates the switching signals, which are then applied to the converter at the specified time instants.

⁸To ensure that OPPs in the experimental setup affect the PCC current and voltage in the same way as in the model of Fig. 1, they are computed assuming $L_d = L_g$, both set to twice the grid inductance of the experimental setup.

TABLE I: Rated values of the system

Parameter	Symbol	SI Value
Voltage	V_R	400 V
Current	I_R	16 A
Angular grid frequency	ω_{gR}	$2\pi 50$ rad/s
Short-circuit ratio	k_{sc}	12.22

TABLE II: System parameters

Grid	Inductance	L_g	5 mH
	Resistance	R_g	100 m Ω
LCL filter	Converter-side inductance	L_{fc}	6.4 mH
	Converter-side resistance	R_{fc}	150 m Ω
	Capacitance	C	10 μ F
	Capacitor resistance	R_c	1 Ω
	Grid-side inductance	L_{fg}	5.8 mH
	Grid-side resistance	R_{fg}	220 m Ω
Converter	Dc-link voltage	V_{dc}	650 V

The selected operating point corresponds to a modulation index of $m = 1.079$, which lies within the typical operation range of $m \in [1, 1.1]$ for grid-connected converters. OPPs with $d = 10$ are considered, resulting in a switching frequency of $f_{sw} = 1050$ Hz, given the rated frequency specified in Table I. For a fair comparison, all benchmarked modulation schemes are designed to operate at the same switching frequency. Accordingly, for SHE, all non-triplen odd harmonics within $n \in [5, 29]$ are eliminated.

To enable a quantitative assessment of compliance with harmonic grid standards [1] and [2], and facilitate a fair comparison across the considered modulation schemes, the following current I_m and voltage V_m metrics are introduced

$$I_m = \frac{1}{2|\mathbb{N}_1|} \sum_{n=5,7,\dots,49} \frac{\max_{\xi_n \in \hat{\xi}_n} (\hat{i}_{pcc,a,n} - \hat{i}_{n,\max})}{\hat{i}_{n,\max}}$$

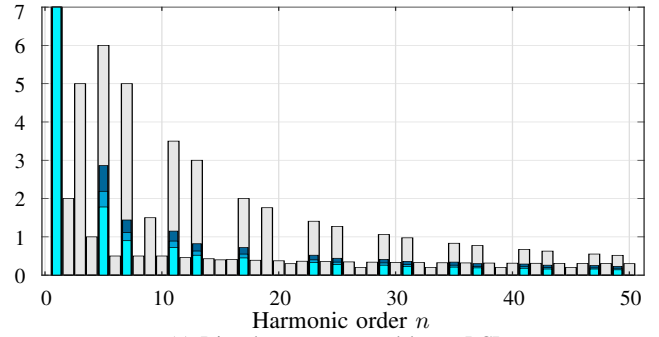
$$V_m = \frac{1}{2|\mathbb{N}_1|} \sum_{n=5,7,\dots,49} \frac{\max_{\xi_n \in \hat{\xi}_n} (\hat{v}_{pcc,a,n} - \hat{v}_{n,\max})}{\hat{v}_{n,\max}},$$

where lower values indicate better compliance. The factor $2|\mathbb{N}_1| = 16$ corresponds to the number of non-triplen odd harmonics over which constraints (16e) and (16f) are enforced in the OPP problem (16). It is noteworthy that the proposed OPP framework is not limited to specific grid standards; alternative standards can be adopted simply by modifying the harmonic limits $\hat{i}_{n,\max}$ and $\hat{v}_{n,\max}$.

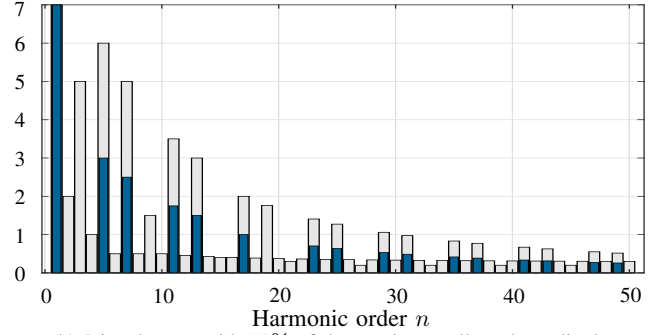
In the sequel, the aforementioned PWM schemes are evaluated under different disturbance profiles.

A. LCI-Generated Disturbance Profile

To evaluate the performance of the considered PWM schemes in a realistic scenario, a three-phase line-commutated inverter (LCI) is assumed to be connected to the PCC. The LCI generates the harmonic disturbances shown by the blue bars in Fig. 7(a). Based on these disturbances, the DA OPPs are designed for the nominal disturbance profile, while the RDA OPPs account for $\pm 25\%$ variations in L_d and R_d . For this scenario, the resulting three-phase PCC current and voltage



(a) Disturbances generated by an LCI.



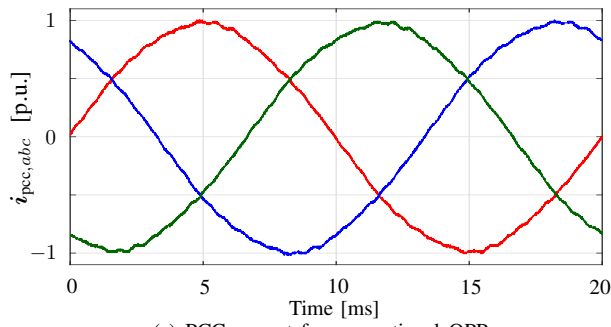
(b) Disturbances with 50% of the maximum allowed amplitudes.

Fig. 7: Harmonic voltage disturbances at the PCC (%) (a) generated by an LCI, (b) with 50% of the maximum allowed amplitudes. In (a), nominal disturbances are shown with blue bars, while the minimum and maximum disturbances resulting from $\pm 25\%$ variations in L_d and R_d are shown with light and dark blue bars, respectively. Grid standard limits are indicated by light gray bars.

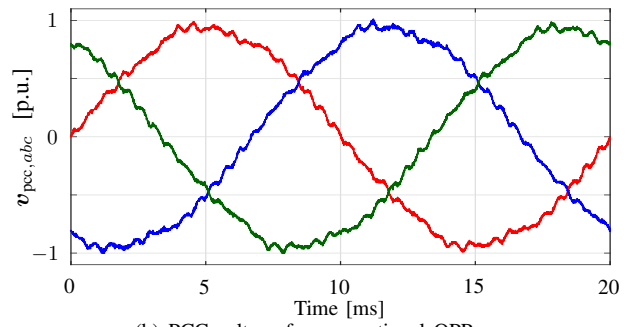
waveforms over one fundamental period (in per unit, p.u.), together with their harmonic spectra, are depicted in Figs. 8 and 9, respectively, for all benchmarked modulation methods. Note that the 19th disturbance harmonic—i.e., the one near the filter resonance frequency—is assumed to be attenuated by a controller.

As can be seen from the time-domain PCC current waveform in Fig. 8(g) and the corresponding harmonic spectrum in Fig. 9(g), the use of RDAG OPPs effectively mitigates the impact of disturbances at the PCC, albeit at the cost of an increased PCC current TDD. In Fig. 9, both numerical and experimental results are presented to demonstrate the accuracy of the experimental tests. Small discrepancies between the numerical and experimental results can be observed, with the most pronounced occurring at the 17th harmonic, i.e., at the system resonance frequency when the grid impedance is considered. These discrepancies arise from mismatches between the nominal and actual system parameters, non-idealities of the experimental setup, and minor asymmetries within the system. These asymmetries also produce low-order harmonics of small amplitude, including triplen and even components.

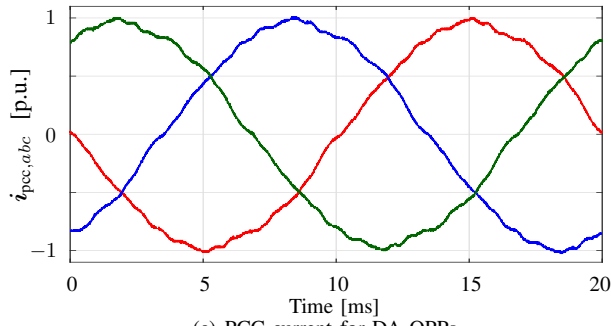
As seen in Fig. 9, all harmonic-constrained HWS OPPs ensure compliance with the current and voltage harmonic limits, even though the disturbance profile is only partially known for the RDA OPPs and completely unknown for the RDAG OPPs. Consequently, the introduced performance metrics yield $I_m = 0$ and $V_m = 0$ for all HWS-based OPPs. In contrast, both conventional OPPs and SHE lead to



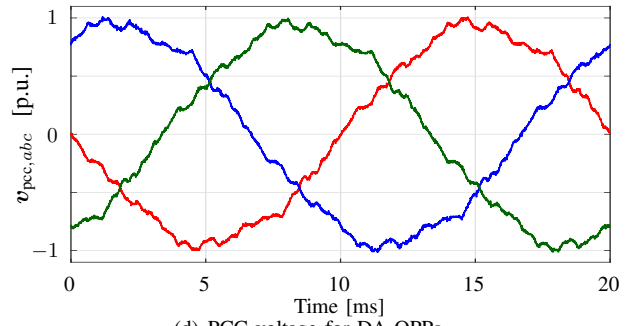
(a) PCC current for conventional OPPs.



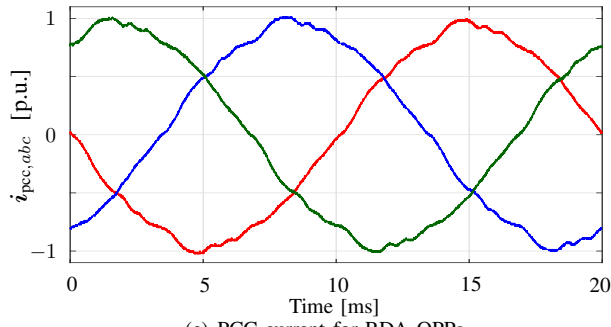
(b) PCC voltage for conventional OPPs.



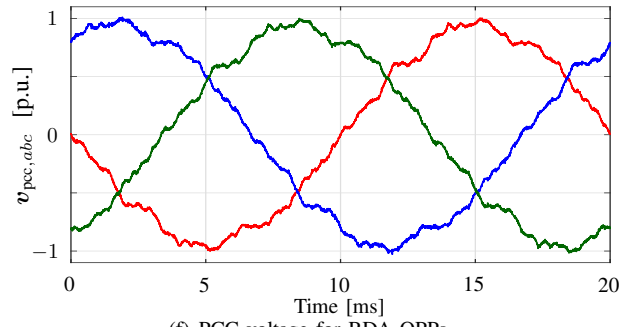
(c) PCC current for DA OPPs.



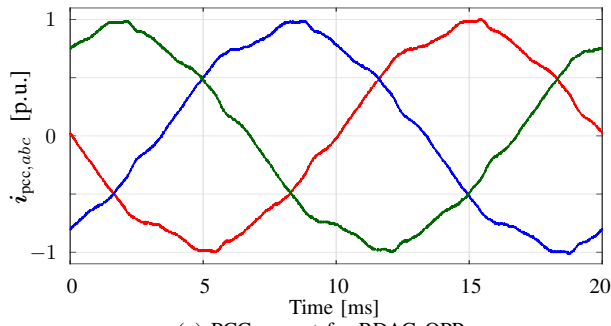
(d) PCC voltage for DA OPPs.



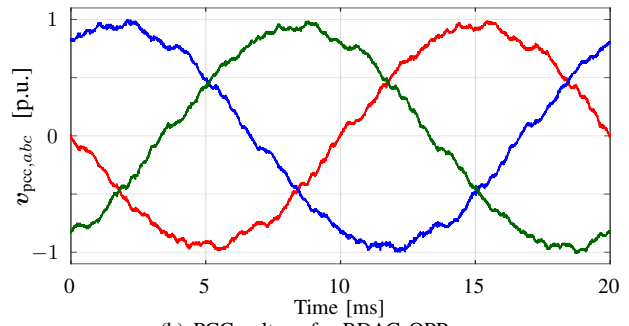
(e) PCC current for RDA OPPs.



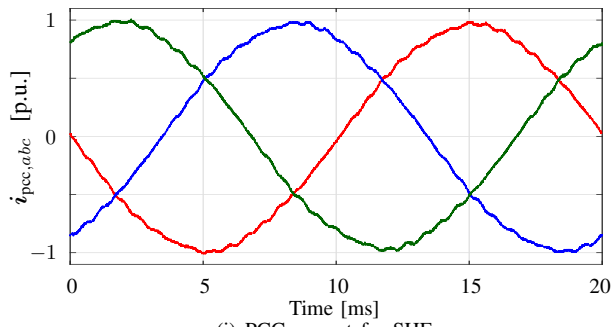
(f) PCC voltage for RDA OPPs.



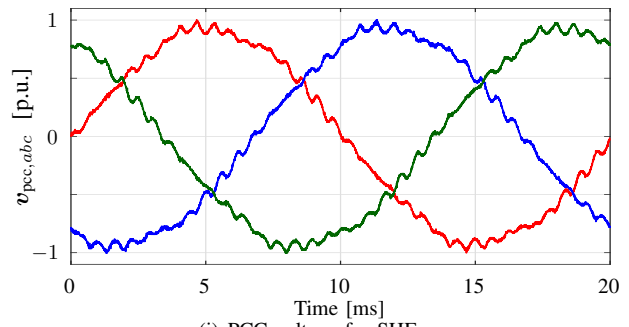
(g) PCC current for RDAG OPPs.



(h) PCC voltage for RDAG OPPs.



(i) PCC current for SHE.



(j) PCC voltage for SHE.

Fig. 8: Three-phase PCC current and voltage under harmonic voltage disturbances generated by an LCI.

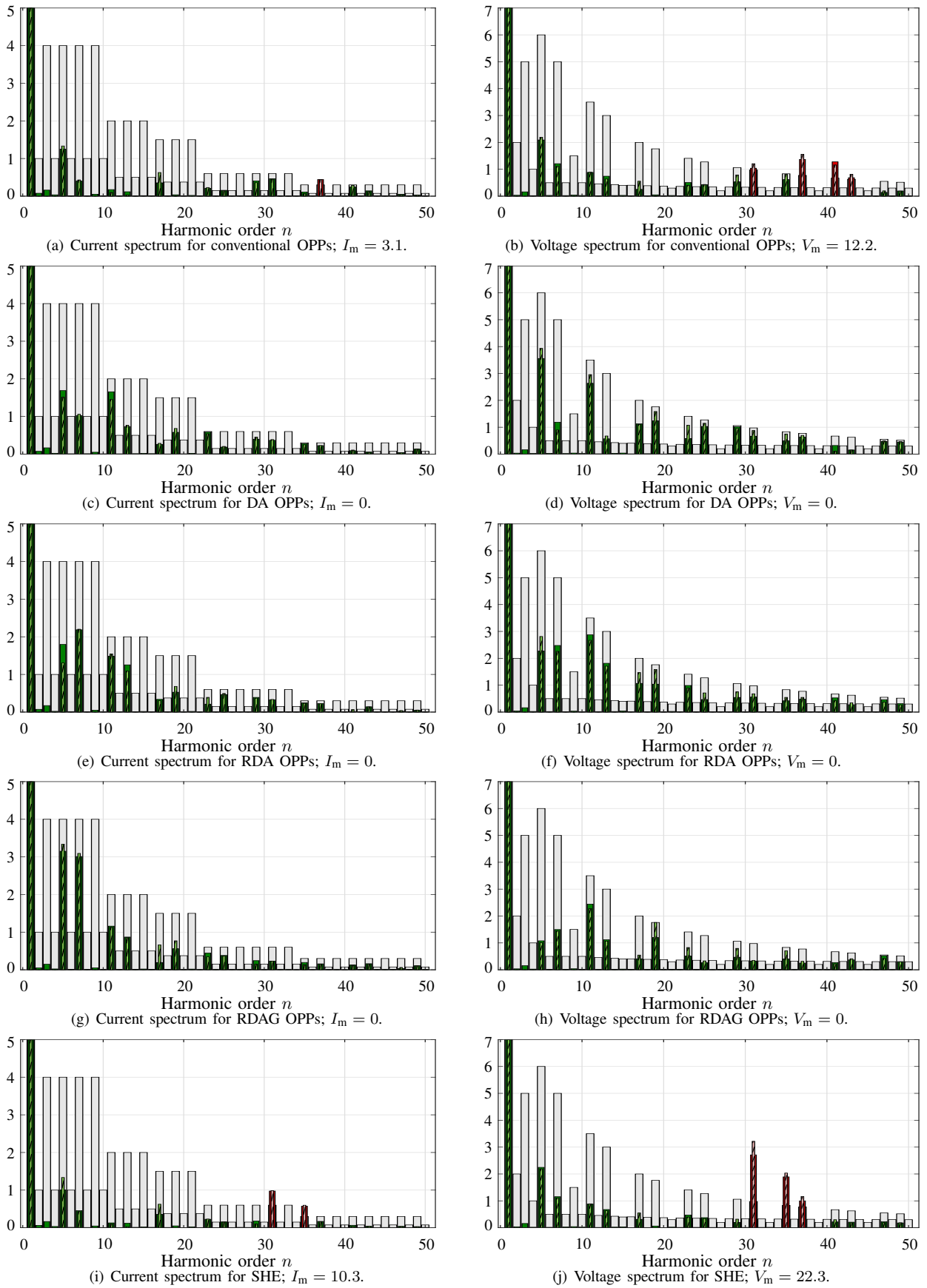


Fig. 9: Current and voltage harmonics at the PCC (in %) under harmonic voltage disturbances generated by an LCI. Grid standard limits are shown as light gray bars, harmonics that comply with them appear in green, and harmonics that violate them in red. Experimental results are indicated by darker, thicker bars, whereas numerical results are shown with lighter, thinner (hatched) bars.

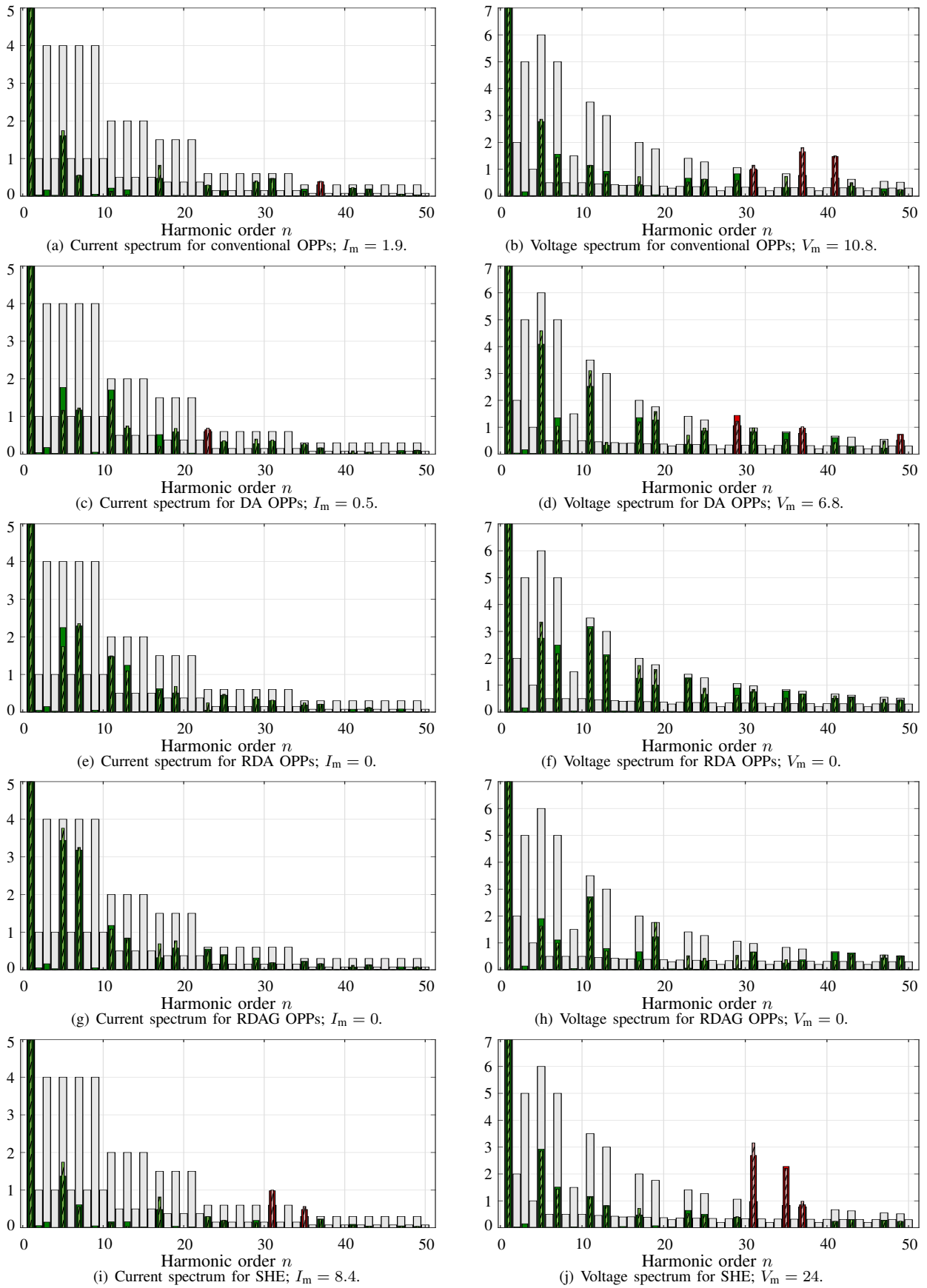


Fig. 10: Current and voltage harmonics at the PCC (in %) under bounded variations in an LCI-induced disturbance profile. Grid standard limits are shown as light gray bars, harmonics that comply with them appear in green, and harmonics that violate them in red. Experimental results are indicated by darker, thicker bars, whereas numerical results are shown with lighter, thinner (hatched) bars.

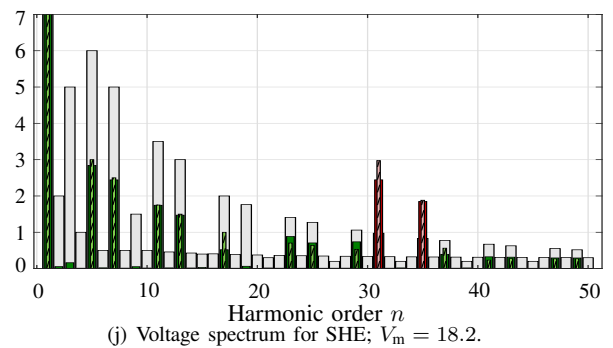
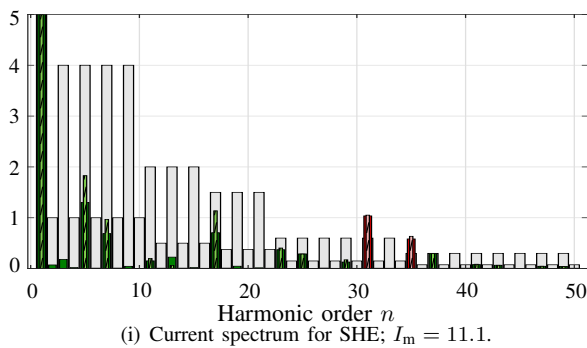
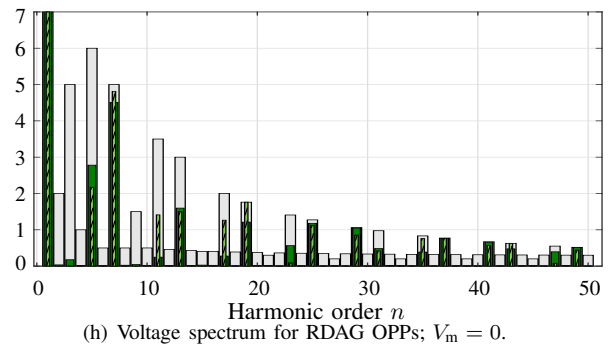
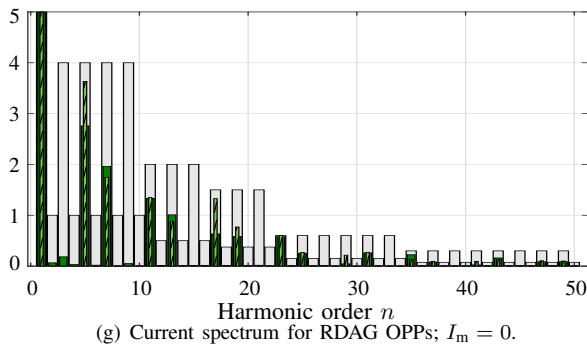
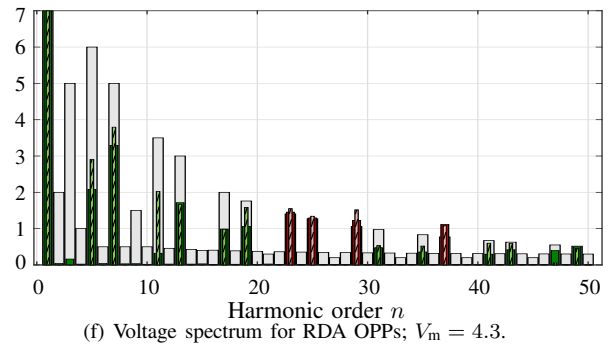
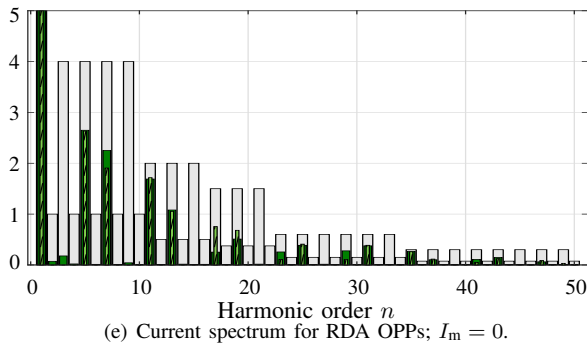
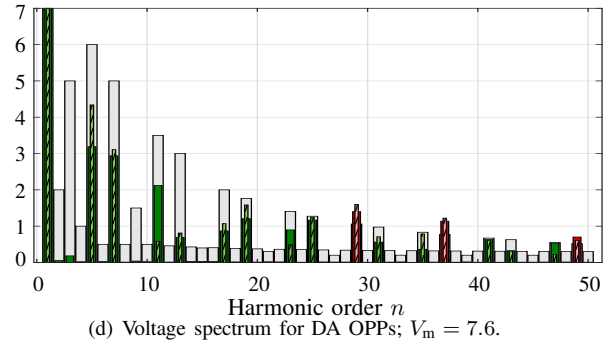
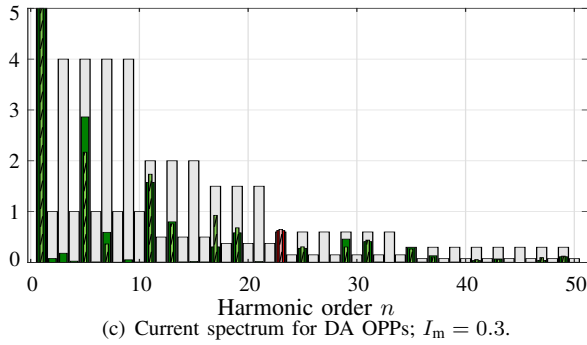
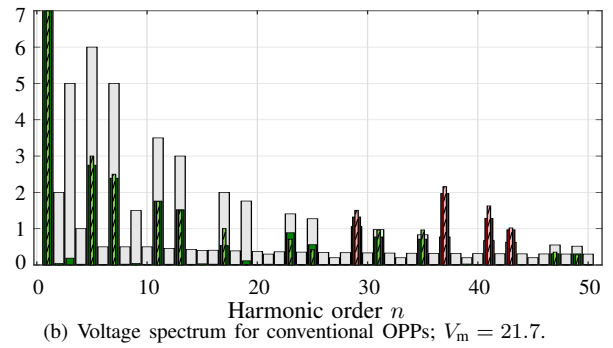
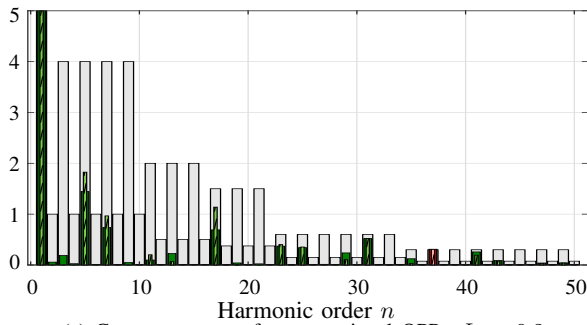


Fig. 11: Current and voltage harmonics at the PCC (in %) under harmonic voltage disturbances with 50% of the maximum allowed amplitudes. Grid standard limits are shown as light gray bars, harmonics that comply with them appear in green, and harmonics that violate them in red. Experimental results are indicated by darker, thicker bars, whereas numerical results are shown with lighter, thinner (hatched) bars.

multiple violations of harmonic standards, reflected in non-zero metrics: $I_m = 3.1$, $V_m = 12.2$ for the conventional OPPs, and $I_m = 10.3$, $V_m = 22.3$ for SHE. These violations are particularly pronounced in the voltage spectra, where harmonics injected by the converter are amplified by the LCI-induced harmonics, resulting in high V_m values.

B. Bounded Variations in LCI-Generated Disturbance Profile

In the presence of bounded variations in the LCI-generated disturbance profile (Fig. 7(a)), the harmonic performance of the benchmarked PWM schemes is shown in Fig. 10. Under such condition, conventional OPPs, SHE, and even DA OPPs (designed for a specific disturbance profile) fail to guarantee full compliance with harmonic grid standards, as indicated by the nonzero values of the compliance metrics I_m and V_m . Nevertheless, DA OPPs still outperform both conventional OPPs and SHE. In contrast, the proposed robust OPPs—both RDA and RDAG variants—that explicitly account for uncertainties in the disturbance amplitudes and phases achieve full compliance, yielding $I_m = 0$ and $V_m = 0$. These results confirm that merely accounting for disturbances in the OPP formulation is not sufficient, and robustness must also be incorporated into the optimization procedure to guarantee compliance under uncertainties.

C. Disturbances with 50% Maximum Allowed Amplitudes

Finally, the evaluation is extended to the case where disturbance harmonics have amplitudes equal to 50% of the limits dictated by [2] (see Fig. 7(b)).⁹ As shown in Fig. 11, conventional OPPs, SHE, and DA OPPs all lead to violations of the current and voltage harmonic limits. In addition, although RDA OPPs, which are designed to achieve robustness against variations in the LCI-generated disturbance profile, exhibit superior compliance, certain PCC voltage harmonics still exceed their limits, as also indicated by the nonzero $V_m = 4.3$. This occurs as the disturbance profile in Fig. 7(b) lies outside the variation range considered during the RDA OPP computation. In contrast, OPPs designed under the assumption of completely unknown disturbances (i.e., RDAG OPPs) ensure full compliance with the harmonic grid standards.

In summary, RDA and RDAG OPPs with embedded robustness outperform conventional programmed PWM schemes, providing improved compliance with harmonic grid standards in the presence of disturbance harmonics at the PCC. However, achieving full compliance when no prior disturbance information is available requires defining sufficiently large uncertainty sets, as discussed in Section III-D.

⁹When RDAG OPPs are computed for the most challenging scenario—i.e., all disturbance harmonics at the maximum amplitudes specified by [2]—it becomes physically impossible to keep all PCC current and voltage harmonics within their respective limits. For the system parameters in Table II, full compliance with both current and voltage harmonic standards under unknown disturbances can only be guaranteed if the disturbance voltage harmonics are restricted to 50% of the maximum allowable amplitudes (see Fig. 7(b)). This limitation arises because, particularly at low harmonic frequencies, mitigating large disturbance voltages requires the converter to inject harmonic voltages that generate current harmonics in phase with the disturbance-induced current harmonics (see Fig. 3). Consequently, these current components add constructively, making it impossible to simultaneously satisfy both PCC voltage and current harmonic limits.

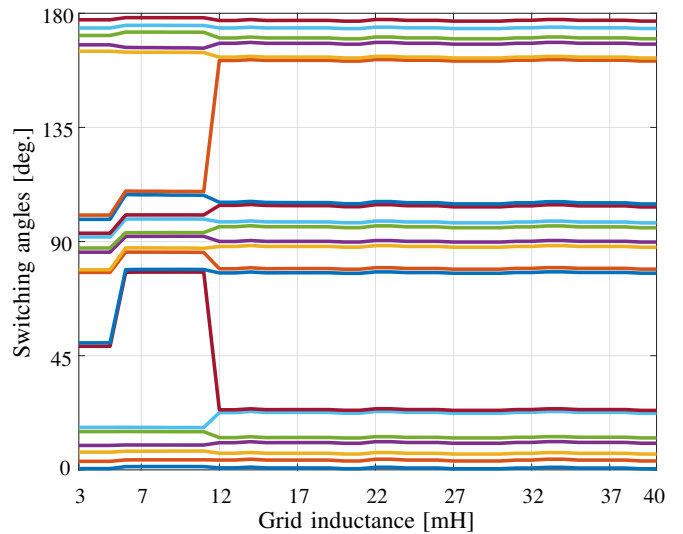


Fig. 12: Primary switching angles (in degrees) of RDAG OPPs for $d = 10$ and $m = 1.079$ as a function of the grid inductance L_g varying from 3 to 40 mH, corresponding to an SCR range of 20.3–1.5.

V. DISCUSSION

Although the proposed robust OPPs facilitate compliance with harmonic grid standards under the assumed bounded disturbances, their emphasis on robustness inevitably leads to higher current and voltage TDDs compared with conventional OPPs computed without considering disturbances. This stems from the conservative nature of the robust design. For example, when disturbance phases are unknown, the optimization framework must consider the full range $[-\pi, \pi)$. Consequently, the phases of the OPP harmonics cannot be selectively adjusted to mitigate specific disturbances, reducing the degrees of freedom available. Additionally, because the converter must inject harmonics in a way that ensures compliance under the most challenging disturbance amplitudes, robust OPPs typically exhibit higher TDDs than DA OPPs under less demanding operating scenarios.

To achieve near-optimal performance across a broad range of scenarios, one option is to precompute multiple disturbance-aware OPPs tailored to different disturbance profiles. However, storing all such patterns in LUTs imposes significant memory requirements, which may hinder practical implementation. This limitation makes adaptive strategies attractive, e.g., real-time OPP generation using learning-based methods may be an alternative for dynamically computing OPPs under disturbances.

Moreover, it is worth mentioning that the computed RDAG OPPs exhibit only limited sensitivity to variations in grid strength, characterized by the short-circuit ratio (SCR). This behavior is illustrated in Fig. 12, which shows that the primary switching angles vary only mildly over a wide SCR range. Consequently, a small set of RDAG OPPs precomputed for representative SCR values and stored in LUTs is sufficient to ensure robust performance across a wide range of practical grid conditions.

VI. CONCLUSIONS

This paper presented an offline PWM framework for computing two-level OPPs for grid-connected converters with

an *LCL* filter, explicitly addressing harmonic disturbances caused by other converters connected to the same PCC. To capture the effect of such disturbances, a harmonic-domain system model was first developed. Building on this model, a robust harmonic-constrained OPP framework was proposed to guarantee compliance with harmonic grid standards even when there are bounded variations in the disturbance profile. The framework was further extended to handle the challenging case of completely unknown disturbances by considering the maximum allowable disturbance amplitudes and all possible phases. To provide more degrees of freedom for such a complicated design, HWS—rather than QaHWS—was imposed on the switching signals. The effectiveness of the proposed framework was validated through both numerical results and experimental tests. The findings demonstrate that the RDAG OPPs guarantee compliance with harmonic grid standards for PCC disturbances with amplitudes up to 50% of the maximum allowed limits. Compared with SHE, conventional OPPs, and even DA OPPs designed for a deterministic disturbance profile, the proposed robust OPPs achieve superior harmonic performance by ensuring compliance in the presence of uncertain harmonic disturbances at the PCC.

APPENDIX

Given (12), the amplitude of the n^{th} PCC current harmonic can be written as

$$\hat{i}_{\text{pcc},a,n} = \left((f_{1,n} + f_{2,n})^2 + (f_{3,n} + f_{4,n})^2 \right)^{1/2}, \quad (17)$$

where $f_{1,n} = a_n Q_{1,n} + b_n Q_{2,n}$ and $f_{3,n} = -a_n Q_{2,n} + b_n Q_{1,n}$ depend on the OPP switching angles, while $f_{2,n} = \tilde{a}_n Q_{3,n} + \tilde{b}_n Q_{4,n}$ and $f_{4,n} = -\tilde{a}_n Q_{4,n} + \tilde{b}_n Q_{3,n}$ depend linearly on the disturbance coefficients $(\tilde{a}_n, \tilde{b}_n)$, which form either an annular uncertainty sector or an uncertainty disk for each harmonic n (see Figs. 4 and 5, respectively).

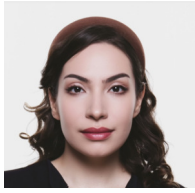
Since $\hat{i}_{\text{pcc},a,n}$ is the Euclidean norm of a two-dimensional affine mapping of $(\tilde{a}_n, \tilde{b}_n)$, it is a convex function of the disturbance coefficients. Therefore, it attains its maximum at the boundary of the uncertainty set, i.e., at the largest admissible disturbance radius.

Since the same reasoning applies to the PCC voltage harmonics in (13), it can be deduced that disturbances with smaller amplitudes cannot yield larger PCC current or voltage harmonics. Hence, this justifies why robust OPPs only need to consider the disturbances with maximum amplitude.

REFERENCES

- [1] IEEE Std 519-2014 (Revision of IEEE Std 519-1992), "IEEE recommended practices and requirements for harmonic control in electrical power systems," pp. 1–29, Jun. 2014.
- [2] IEC Std 61000-2-4, "Electromagnetic compatibility (EMC)—part 2-4: Environment—compatibility levels in industrial plants for low-frequency conducted disturbances," Sep. 2002.
- [3] L. A. Moran, J. W. Dixon, and R. R. Wallace, "A three-phase active power filter operating with fixed switching frequency for reactive power and current harmonic compensation," *IEEE Trans. Ind. Electron.*, vol. 42, no. 4, pp. 402–408, Aug. 1995.
- [4] D. Bernet, L. Stefanski, and M. Hiller, "Integrating voltage-source active filters into grid-connected power converters—modeling, control, and experimental verification," *IEEE Trans. Power Electron.*, vol. 36, no. 11, pp. 12 218–12 233, Apr. 2021.

- [5] P. Acuña, L. Morán, M. Rivera, J. Dixon, and J. Rodríguez, "Improved active power filter performance for renewable power generation systems," *IEEE Trans. Power Electron.*, vol. 29, no. 2, pp. 687–694, Apr. 2014.
- [6] D. G. Holmes and T. A. Lipo, *Pulse width modulation for power converters: Principles and practice*. Piscataway, NJ, USA: IEEE Press, 2003.
- [7] M. S. A. Dahidah, G. Konstantinou, and V. G. Agelidis, "A review of multilevel selective harmonic elimination PWM: Formulations, solving algorithms, implementation and applications," *IEEE Trans. Power Electron.*, vol. 30, no. 8, pp. 4091–4106, Aug. 2015.
- [8] J. Nápoles, J. I. Leon, R. Portillo, L. G. Franquelo, and M. A. Aguirre, "Selective harmonic mitigation technique for high-power converters," *IEEE Trans. Ind. Electron.*, vol. 57, no. 7, pp. 2315–2323, Jul. 2010.
- [9] J. Pontt, J. Rodríguez, and R. Huerta, "Mitigation of noneliminated harmonics of SHEPWM three-level multipulse three-phase active front end converters with low switching frequency for meeting standard IEEE-519-92," *IEEE Trans. Power Electron.*, vol. 19, no. 6, pp. 1594–1600, Nov. 2004.
- [10] A. Moeini, H. Iman-Eini, and M. Bakhshizadeh, "Selective harmonic mitigation—pulse-width modulation technique with variable dc-link voltages in single and three-phase cascaded H-bridge inverters," *IET Power Electron.*, vol. 7, no. 4, pp. 924–932, Apr. 2014.
- [11] J. Nápoles, A. J. Watson, J. J. Padilla, J. I. León, L. G. Franquelo, P. W. Wheeler, and M. A. Aguirre, "Selective harmonic mitigation technique for cascaded H-bridge converters with nonequal dc link voltages," *IEEE Trans. Ind. Electron.*, vol. 60, no. 5, pp. 1963–1971, May 2013.
- [12] M. Najjar, A. Moeini, M. K. Bakhshizadeh, F. Blaabjerg, and S. Farhangi, "Optimal selective harmonic mitigation technique on variable dc link cascaded H-bridge converter to meet power quality standards," *IEEE J. Emerg. Sel. Topics Power Electron.*, vol. 4, no. 3, pp. 1107–1116, Sept. 2016.
- [13] A. Moeini, H. Zhao, and S. Wang, "A current-reference-based selective harmonic current mitigation PWM technique to improve the performance of cascaded H-bridge multilevel active rectifiers," *IEEE Trans. Ind. Electron.*, vol. 65, no. 1, pp. 727–737, Jan. 2018.
- [14] G. S. Buja and G. B. Indri, "Optimal pulswidth modulation for feeding ac motors," *IEEE Trans. Ind. Appl.*, vol. IA-13, no. 1, pp. 38–44, Jan./Feb. 1977.
- [15] L. G. Franquelo, J. Nápoles, R. C. P. Guisado, J. I. León, and M. A. Aguirre, "A flexible selective harmonic mitigation technique to meet grid codes in three-level PWM converters," *IEEE Trans. Ind. Electron.*, vol. 54, no. 6, pp. 3022–3029, Dec. 2007.
- [16] A. Birda, J. Reuss, and C. M. Hackl, "Synchronous optimal pulswidth modulation for synchronous machines with highly operating point dependent magnetic anisotropy," *IEEE Trans. Ind. Electron.*, vol. 68, no. 5, pp. 3760–3769, May 2021.
- [17] A. K. Rathore, J. Holtz, and T. Boller, "Synchronous optimal pulswidth modulation for low-switching-frequency control of medium-voltage multilevel inverters," *IEEE Trans. Ind. Electron.*, vol. 57, no. 7, pp. 2374–2381, Jul. 2010.
- [18] J. A. Pontt, J. R. Rodríguez, A. Liendo, P. Newman, J. Holtz, and J. M. S. Martin, "Network-friendly low-switching-frequency multipulse high-power three-level PWM rectifier," *IEEE Trans. Ind. Electron.*, vol. 56, no. 4, pp. 1254–1262, Apr. 2009.
- [19] V. G. Monopoli, A. M. Alcaide, L. Bruno, G. Rendine, J. I. Leon, M. Liserre, and L. G. Franquelo, "Hybrid modulation technique for operating medium-voltage high-power CHB converters under grid voltage disturbances," *IEEE Trans. Ind. Electron.*, vol. 71, no. 1, pp. 462–472, Feb. 2024.
- [20] S. Rahmanpour, P. Karamanakos, and T. Geyer, "Harmonic-constrained three-level optimized pulse patterns for grid-connected converters with *LCL* filters," *IEEE Trans. Ind. Appl.*, vol. 61, no. 5, pp. 7481–7492, Sep./Oct. 2025.
- [21] —, "Optimized pulse patterns for converters connected to a distorted grid via *LCL* filters," in *Proc. IEEE Energy Convers. Congr. Expo. Europe*, Darmstadt, Germany, Sep. 2024, pp. 1–8.
- [22] A. Birth, T. Geyer, H. d. T. Mouton, and M. Dorfling, "Generalized three-level optimal pulse patterns with lower harmonic distortion," *IEEE Trans. Power Electron.*, vol. 35, no. 6, pp. 5741–5752, Jun. 2020.



Shirin Rahmanpour (Student Member, IEEE) received the B.S. and M.S. degrees in electrical engineering-control from the Sahand University of Technology, Tabriz, Iran, in 2014, and 2018, respectively.

Since 2022, she has been with the Faculty of Information Technology and Communication Sciences, Tampere University, Tampere, Finland, where she is currently working toward the Ph.D. degree in computing and electrical engineering. Her main research interests include optimal modulation, mathematical programming, and power electronics.

emational programming, and power electronics.



Petros Karamanakos (Senior Member, IEEE) received the Diploma and Ph.D. degrees in electrical and computer engineering from the National Technical University of Athens (NTUA), Athens, Greece, in 2007, and 2013, respectively.

From 2010 to 2011, he was with the ABB Corporate Research Center, Baden-Dättwil, Switzerland, where he worked on model predictive control strategies for medium-voltage drives. From 2013 to 2016, he was a PostDoc Research Associate in the Chair of Electrical Drive Systems and Power Electronics,

Technische Universität München, Munich, Germany. Since 2016, he has been with the Faculty of Information Technology and Communication Sciences, Tampere University, Tampere, Finland, where he is currently an Associate Professor. His main research interests lie at the intersection of power electronics, optimal control, mathematical programming, and computational methods, including model predictive control and optimal modulation for utility-scale power converters and ac variable speed drives.

Dr. Karamanakos has received three IEEE journal paper awards and five prize paper awards at IEEE conferences. He serves as an Associate Editor of the IEEE Transactions on Power Electronics, IEEE Journal of Emerging and Selected Topics in Power Electronics, IEEE Transactions on Industry Applications, and IEEE Open Journal of Industry Applications. He has been a Regional Distinguished Lecturer of the IEEE Power Electronics Society since 2022.



Tobias Geyer (Fellow, IEEE) received the Dipl.-Ing. degree in electrical engineering, the Ph.D. degree in control engineering, and the Habilitation degree in power electronics from ETH Zurich, Zurich, Switzerland, in the years 2000, 2005 and 2017, respectively.

After his Ph.D., he spent three years at GE Global Research, Munich, Germany, three years at the University of Auckland, Auckland, New Zealand, and eight years at ABB's Corporate Research Centre, Baden-Dättwil, Switzerland. In 2020, he joined

ABB's Medium-Voltage Drive division as R&D Platform Manager of the ACS6000 and ACS6080. In 2022, he became a Corporate Executive Engineer. He has been an extraordinary Professor at Stellenbosch University, Stellenbosch, South Africa, since 2017.

He is the author of more than 40 patent families, 170 publications, and the book "Model predictive control of high power converters and industrial drives" (Wiley, 2016). He teaches a regular course on model predictive control at ETH Zurich. His research interests include medium-voltage and low-voltage drives, utility-scale power converters, optimized pulse patterns and model predictive control.

Dr. Geyer received the IEEE IAS Gerald Kliman Innovator Award in 2025, the IEEE PELS Modeling and Control Technical Achievement Award in 2022, the Semikron Innovation Award in 2021, and the Nagamori Award in 2021. He also received two Prize Paper Awards of IEEE Transactions and four Prize Paper Awards at IEEE conferences. He is a former Associate Editor of the IEEE Transactions on Industry Applications (from 2011 until 2014) and the IEEE Transactions on Power Electronics (from 2013 until 2019). He was an International Program Committee Vice Chair of the IFAC conference on Nonlinear Model Predictive Control in Madison, WI, USA, in 2018. Dr. Geyer was a Distinguished Lecturer of the IEEE Power Electronics Society from 2020 to 2023.



Arttu Ruusila (Student Member, IEEE) received the B.S. degree in electrical engineering from Lappeenranta-Lahti University of Technology LUT, Lappeenranta, Finland, in 2021, and the M.S. degree in automation engineering from Tampere University, Tampere, Finland, in 2023, where he is currently pursuing the Ph.D. degree with the Faculty of Information Technology and Communication Sciences.

His research interests include model predictive control and control of grid-connected converters.



George Papafotiou (Member, IEEE) received the Diploma and Ph.D. degrees in electrical engineering from the Aristotle University of Thessaloniki, Thessaloniki, Greece, in 1997, and 2002, respectively.

From 2003 to 2006, he was with the Automatic Control Laboratory, ETH Zurich, Zurich, Switzerland, where he was working on model predictive control for hybrid systems, with a special focus on dc-dc converters and induction motor drives. From 2006 to 2012, he was with the ABB Corporate Research Center, Dättwil, Switzerland, where he was

working on the development of modern control and estimation methods for power electronics applications, and after 2010 leading the Power Electronics Systems Team. From 2012 to 2017, he was responsible for the global R&D activities in control SW and control HW for ABB's MV Drives, and from 2017 to 2021, he was Quality and Customer Experience Manager for the System Drives Division of ABB Motion.

In 2021, he joined the Electromechanics and Power Electronics group at the Eindhoven University of Technology, where he is currently leading the Power Electronics Lab. His current research interests are in the area of employing computational intelligence for reliability and resilience of power electronics systems.